Multiobjective Optimization of an Industrial Ethylene Reactor Using a Nondominated Sorting Genetic Algorithm

Abhijit Tarafder, Bennett C. S. Lee, Ajay K. Ray, and G. P. Rangaiah*

Department of Chemical and Biomolecular Engineering, National University of Singapore, 10 Kent Ridge Crescent, Singapore 119206, Singapore

Ethylene is produced in the largest volume among the monomers, and hence, any improvement in its production process can bring important benefits to both industry and consumers. In the present paper, an industrial ethylene reactor has been studied with a multiobjective optimization technique to find a scope for further improvements and to detect a range of optimal solutions. An industrial reactor unit using ethane as the feedstock was modeled, assuming a detailed free-radical mechanism for the reaction kinetics coupled with material, energy, and momentum balances of the reactant−product flow along the reactor. To carry out the multiobjective optimization for two and three objectives, the elitist nondominated sorting genetic algorithm, or NSGA-II, was chosen. Instead of a single optimum as in traditional optimization, a broad range of optimal design and operating conditions depicting tradeoffs of key performance parameters such as conversion, selectivity and ethylene flow rate was successfully obtained. The effects of design and operating variables on the optimal solutions are discussed in detail, and the generated results are compared with industrial data.

1. Introduction

Ethylene monomer is one of the base petrochemicals that form the building blocks of the petrochemical industry and is produced in the largest volume among them. In 2001, the global production of ethylene amounted to 90.4 million metric tons, valued at an estimated $60 billion (in U.S. dollars),[1] and by 2005, the annual global production will reach 104 million metric tons, with an estimated growth rate of 4% per year.[2] The bulk of ethylene produced is used in the production of plastics, primarily polyethylene. Moreover, it is an ideal base material for many other petrochemicals, as it is readily available at low cost and high purity and usually reacts with other low-cost materials, such as oxygen and water. From the above data, it can be perceived that even a small improvement in the processing of ethylene has the potential of bringing a high-dividend to the petrochemical industry. This paper presents a multiobjective optimization study carried out to find a range of better operating conditions for improving the performance of ethylene production units based on ethane feed. This is perhaps the first study on multiobjective optimization of an ethylene reactor. The rest of this section briefly reviews ethylene production; modeling of an ethylene reactor; and multiobjective optimization, including the methods used in this study.

Ethylene Production. Ethylene is usually produced through the steam cracking of feedstocks such as ethane, naphtha, or gas oil.[3] The choice of feedstock is an important economic decision as it influences other costs as well. Subject to availability, ethane is probably the best feedstock, as it has higher yield and selectivity of ethylene than heavier feedstocks and its processing is relatively simple, involving lower capital costs. Steam cracking is an endothermic process leading to the breaking up of large molecules into smaller ones. The
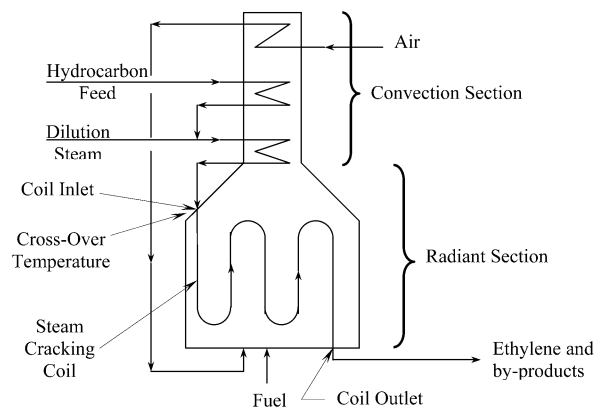

Figure 1. Simplified sketch of a typical furnace for the steam cracking of hydrocarbons.

cracking process is carried out in long tubular reactors, known as radiant tubes, which are placed vertically in a large, rectangular gas-fired furnace.[4] The furnace consists of convection and radiation sections (Figure 1), where the feedstock first enters the convection section so that the hot stack gas preheats the feed before it enters the radiation section. Typical inlet temperatures to the radiant tube range from 500 to 800 °C.[4] At an intermediate point in the convection section, steam is introduced and is preheated together with the feedstock. Steam lowers the partial pressure of high-molecular-mass aromatics, reducing condensation reactions; in addition, it contributes to the partial removal of coke in the tubes. The radiant coil is directly heated by the burners, leading the process gas to the cracking temperature, which ranges from 700 to 900 °C. The temperature at the outlet of the radiant coil typically ranges from 775 to 885 °C.[3] The reactor effluent is quickly quenched to prevent further reaction; compressed; and sent to a separation unit for the recovery of ethylene and other products such as methane, ethane, propane, propylene, butylenes, and pyrolysis gasoline.

---

* To whom correspondence should be addressed. Tel.: (65) 68742187. Fax: (65) 67791936. E-mail: chegpr@nus.edu.sg.

Reaction Mechanism and Modeling of Steam Cracker. The reaction mechanism of steam cracking of hydrocarbons to form ethylene can be formulated in different ways, namely, according to overall, molecular, and free-radical mechanisms, of which the last is the most detailed and perhaps the most accurate.[4] Froment et al.[5,6] proposed molecular schemes approximating the free-radical nature of ethane cracking, where kinetic parameters were estimated on the basis of pilot-plant data. These models are easier to solve because they lead to a set of nonstiff differential equations, whereas the free-radical mechanism leads to stiff differential equations that are difficult to solve.[7] Sundaram and Froment[8] developed a free-radical scheme for ethane cracking, where 49 reactions were proposed and products heavier than C_5H_{10}, whose yields are usually very small, were lumped together as the single component C_{5+} to simplify the reaction scheme. Kinetic parameters were mainly obtained through trial and error and by fitting pilot-plant data. Other free-radical schemes have also been proposed by several authors, using fewer reactions.[9,10] Rangaiah et al.[11] evaluated several reaction schemes for ethane cracking, including the molecular[6] and the free-radical schemes[8] by Froment and his group, and concluded that the free-radical mechanism of Sundaram and Froment[8] provides more accurate predictions.

Modeling the ethylene reactor, including the steam cracking reactions, can be very complex; however, certain assumptions simplify the task. The mass flow inside the reactor, which has a large length-to-diameter ratio and a high fluid velocity,[12] can be taken as plug flow. The heat transfer from the furnace gases to the cracking reactor can be represented by a heat-flux profile, thus uncoupling the reactions and thermal phenomena occurring inside the tubes from those occurring outside. Froment et al.[5] successfully simulated a steam cracker to study the cracking of ethane and ethane−propane mixtures. By using an independently simulated heat-flux profile, a good agreement with industrial data was achieved. A one-dimensional model was used for the mass, momentum, and heat-transfer equations, as high turbulence in the reactor tubes would effectively cancel out any flow profile over the cross section.[13] The external heat-flux profile is an important factor in the cracking reaction, and there are successful models of the mechanism[14,15] investigating the effects of different firing patterns on the reaction temperature and product distribution. However, it was argued that, to predict solely the effluent yield, an accurate heat-flux profile is not crucial.[16]

Multiobjective Optimization. The real-life optimization problems faced in industry usually deal with more than one competing objective. Traditionally, solving such problems involves taking a weighted average of all of the objectives and treating it as a single-objective optimization problem. However, the solution then depends on the chosen weights, which, in turn, are subject to individual perception and knowledge of the process. This is quite arbitrary, and a deficiency is always inherent in this method.[17] The best way to solve and represent the solution of a multiobjective optimization problem is through the generation of a Pareto-optimal set,[18] which provides a spectrum of tradeoffs of the competing objectives. All of the solutions in a Pareto-optimal set are equally good, i.e., none of them is better than the others in the set unless another criterion is supplied to compare them. A Pareto-optimal set provides a wide range of design and operational options to designers and practitioners and, hence, enhances the possibility of finding more efficient processes. Population-based algorithms, such as genetic algorithms (GAs), have the capability of finding a Pareto-optimal set in a single run with only a marginal increase in the computational time.

GA is a search technique based on the working principles of genetics and natural selection; it employs a population-based approach whereby the search for a solution is performed with a group of estimated solutions rather than a single one. Starting with a *set* of randomly generated initial estimates of independent variables, also called decision variables, GA tries to reach the solution with the help of special operators. Each iteration is called a *generation* in which new values of independent variables are found through special operations, namely, reproduction, crossover, and mutation, on their old values. This is done in an attempt to produce more desirable objective values until a preassigned number of generations is computed. Based on the fundamentals of GA, Srinivas and Deb[18] developed the nondominated sorting genetic algorithm (NSGA) to find the Pareto-optimal set of solutions for solving multiobjective optimization problems. Nondomination refers to a solution being better in at least one objective than any other solution in the population. The concept of nondomination, first introduced by Goldberg,[19] is necessary to assign a *fitness* value to each solution that ultimately determines its place in the Pareto-optimal set.

Although NSGA has been successfully applied to many multiobjective optimization problems,[20−23] Deb et al.[24] reported that its computational complexity can be dramatically reduced, and by applying elitism, a method of preserving good solutions, its performance can be still increased. This revision in NSGA resulted in another algorithm, which they named elitist NSGA or NSGA-II. Deb et al.[24] showed that NSGA-II is able to achieve better convergence near the true Pareto-optimal front and find a much better spread of Pareto-optimal solutions. GA operators, designed to be applied to binary numbers, require binary coding for the real values of decision variables. However, it was noted[25] that representing real numbers with binary coding leads to a number of difficulties such as the finite-length binary strings are unable to achieve high precision in the decision variables. Moreover, in some strings, a transition to a neighboring point requires the alteration of many bits, which, in turn, hinders the gradual search in the continuous search space. This is also known as the Hamming cliff problem. To counter these problems, genetic operators that are capable of operating directly on real numbers have been proposed. The simulated binary crossover (SBX) operator proposed by Deb and Agrawal[25] is a successful example. The present authors noted that the SBX operator, which actually mimics the operation of binary crossover, is able to perform as good as or even better than binary-coded GAs.[26] This real-coded operator was also incorporated in NSGA-II.[24] Although binary-coded NSGA-II has been satisfactorily used by other workers in optimizing chemical processes,[27,28] the present study employs real-coded NSGA-II (with the SBX operator) for better results. The authors could find only one contemporary work employing real-coded NSGA-II for a multiobjective optimization study on an epoxy polymerization reactor;[29] better

results were also obtained in this case with real-coded over binary-coded NSGA-II.

2. Modeling and Sensitivity Analysis of the Steam Cracker

In the present study, the industrial steam cracker described by Froment et al.[5] is used as the basis for simulation and optimization of an ethylene reactor for multiple objectives. A multiobjective optimization study with NSGA-II requires execution of the steam cracker model for each member of its population over a certain number of generations. Because the number of population typically ranges from 50 to 100 and the number of generations needed to find a reasonably good Pareto can be more than 200, a typical study involves computation of the steam cracker model 10 000−20 000 times. Such a huge computational load makes the molecular scheme of cracking reactions look more attractive, as it results in nonstiff differential equations and hence requires lower computational times, although obtained in a tradeoff with prediction accuracy. For the current study, however, the free-radical mechanism proposed by Sundaram and Froment[8] was ultimately chosen for reactor modeling. It was perceived that, with the present powerful personal computers, the time penalty can be brought down to a more acceptable level rather than settling for a lower accuracy. The selected free-radical mechanism for ethane cracking consists of 49 reactions with 11 molecular species and 9 free radicals. Details of this scheme can be obtained from the literature,[8] where it was assumed that the reactions are elementary and therefore the order of each reaction corresponds to its molecularity. The molecular and free-radical species and the governing equations of the steam cracker model, including the material, energy, and momentum balances, are listed in Appendix A. The model was validated by comparison with industrial data, as shown in Table A3.

Sensitivity Analysis of the Steam Cracker. A sensitivity analysis was performed with the steam cracker model to note the effects of some key variables, which were identified as the decision variables in the subsequent optimization study on the reactor performance. The variables are the temperature (T_{in}) and pressure (P_{in}) of the ethane−steam mixture at the inlet to the radiation section; the coefficients of the heat-flux profile, α, β, and γ in eq A13, that control the rate of heat input to the cracking reactions; the steam-to-ethane (mass) ratio (SR); the ethane flow rate (F_{in}) to the reactor; the number of tubes (n_{tubes}) defining the reactor length; and the inner diameter of the reactor tubes (d_{in}). The values of each of these variables were varied within a preassigned domain, while the others were kept constant, to note the effects of variation on some calculated quantities that show the reactor performance. These quantities are the conversion (X) of ethane, the selectivity of ethylene ($S_{C_2H_4}$), and the mass flow rate of ethylene ($f_{C_2H_4}$) at the reactor exit, which together define the extent and the quality of reaction process. The ethane conversion and ethylene selectivity were defined as

conversion, $X =$
$$\text{(mass flow rate of pure ethane fed} -$$
$$\text{mass flow rate of pure ethane at exit)/}$$
$$\text{(mass flow of pure ethane fed)} \quad (1)$$

selectivity, $S_{C_2H_4} =$
$$\text{(mass flow rate of ethylene at exit} -$$
$$\text{mass flow rate of ethylene fed)/}$$
$$\text{(mass flow rate of pure ethane fed} -$$
$$\text{mass flow rate of pure ethane at exit)} \quad (2)$$

It is known that any reaction is ultimately controlled by the residence time, temperature, and pressure in the reactor. Hence, the three additional variables residence time, average reaction temperature, and average reaction pressure were calculated along with the performance variables to develop a clearer understanding of the effects of the decision variables. These three variables were calculated in the following way

$$t_r = \int_{x=0}^{L} \frac{\left(\frac{\pi}{4}d_{in}^2\right) dx}{[F_{steam}(x) + \sum_j F_j(x)]\dfrac{RT(x)}{P(x)}} \quad (3)$$

$$T_{avg} = \frac{\int_{x=0}^{L} T(x) \, dx}{L} \quad (4)$$

$$P_{avg} = \frac{\int_{x=0}^{L} P(x) \, dx}{L} \quad (5)$$

The range of each decision variable for sensitivity analysis was determined on the basis of industrial practice and numerical feasibility, a detailed account of which is presented in the next section. The outcome of the entire analysis is presented in Figure 2.

The sensitivity analysis of the inlet temperature shows that an increase in temperature resulted in increased ethane conversion and decreased ethylene selectivity (Figure 2a). The ethylene flow rate, which is favored by high conversion and high selectivity, increased steadily with increasing temperature as the selectivity decreased at a lower rate than the conversion (Figure 2a). The main reason behind the sharp conversion increment is the increase in average reaction temperature and decrease in average pressure (Figure 2a). Low residence time and low pressure improve selectivity, but in the present case, the influence of the high reaction temperature, which reduces selectivity, had a more dominant effect.

On the other hand, the effect of reaction pressure on the cracker performance is not very substantial (Figure 2b). An increase in pressure slightly increased the ethane conversion while decreasing the ethylene selectivity. As the selectivity decreased at a rate similar to the conversion increment, the variation in the ethylene flow rate was negligible. An increase in pressure most prominently influenced the residence time, as can be seen in Figure 2b. It seems that high residence time and high reaction pressure had contradictory effect on the reaction, and so, the variations in the conversion and ethylene flow rate were insignificant.

The heat-flux parameters α, β, and γ in eq A13, when increased, resulted in increased ethane conversion and decreased ethylene selectivity although with different relative effects. The ethylene flow rate increased because the conversion increment was higher than the selectivity decrement (Figure 2c−e). The effect of α was
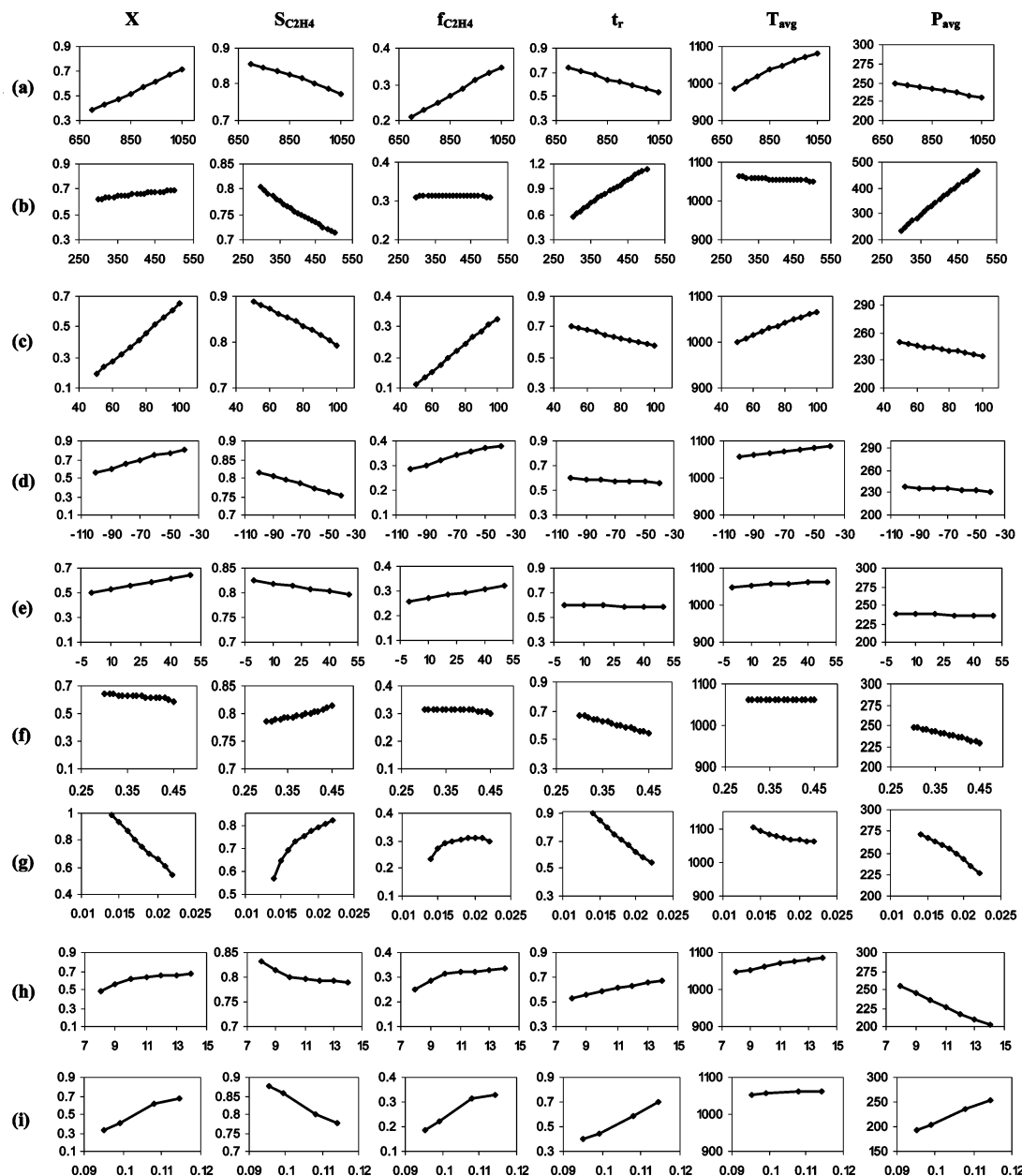
Figure 2. Sensitivity of ethane conversion, ethylene selectivity, ethylene flow rate, residence time, average temperature, and average pressure in the reactor (shown on the y axis) to decision variables (shown on the x axis): (a) inlet temperature (T_{in}); (b) inlet pressure (P_{in}); (c−e) α, β, and γ in the heat-flux profile, respectively; (f) steam-to-ethane ratio (SR); (g) ethane feed rate (F_{in}); (h) number of tubes (n_{tubes}); and (i) tube inner diameter (d_{in}). Note that the ranges of quantities on the y axis are not uniform for all decision variables, but rather are scaled to amplify, for clarity, their variation against the decision variables.

the most prominent among the three parameters. As α increased, the reaction temperature increased sharply, and the residence time decreased. However, as the influence of reaction temperature increment was more dominant than that of the residence time decrement, the net conversion increased substantially.

Steam reduces the reaction pressure in two ways: by acting as a diluent, it decreases the partial pressures of the reactants, and by increasing the overall flow rate through the reactor, it increases the total pressure drop as well. Consequently, as the SR increased, the conversion decreased, and the selectivity increased slightly (Figure 2f), resulting in a marginal decrease of the ethylene flow rate. The net residence time decreased, as the net flow rate through the reactor increased and the reactor dimensions remained the same. Decreases in the residence time and the reaction pressure coun-

teracted each other and resulted in little or insignificant variation of the conversion and ethylene flow rate values.

Increasing the ethane feed rate sharply decreased the conversion (Figure 2g) while increasing the selectivity. The main reason for the former is the sharp decrease in residence time as flow rate increased. The rise in selectivity resulted from the decreased reaction temperature, reaction pressure, and residence time. The ethylene flow rate increased initially because of the initial sharp rise of selectivity; however, it gradually stopped increasing and ultimately decreased because of the sharp fall in ethane conversion.

Increasing the number of tubes or diameter increased the reactor volume and thus the residence time in the reactor (Figure 2h and i). On the other hand, increasing the length resulted in a higher pressure drop along the

reactor, whereas increasing the diameter resulted in a lower pressure drop. The reaction temperature stayed almost invariant when the diameter was increased, whereas it increased when the number of tubes was increased, mainly because of the higher increase in the heat-transfer area. As the number of tubes and diameter increased, higher conversion and lower selectivity values were noted because of the increased residence time and reaction temperature. However, the decrease in pressure as the number of tubes was increased moderated the rate of change of the conversion and selectivity, whereas for the diameter increase, the variations of conversion and selectivity were monotonic.

3. Formulation of the Optimization Problem

For the optimization study of an ethane cracker unit, the objectives depend on production preferences, which are often based on profit. As the profit calculation encompasses several factors, viz., demand and prices that fluctuate with time and location, downstream processing costs, etc., this study selected objectives that increase the scope of making profit rather than maximizing the profit itself. From the reaction point of view, the most pertinent objectives are to maximize the ethylene production and minimize the production of side products. Therefore, the conversion of ethane, selectivity of ethylene, and flow rate of ethylene were chosen as the objectives. In the sensitivity analysis section, it was observed that the conversion and selectivity vary in opposite directions, whereas the ethylene flow rate depends on conversion and selectivity. Hence, initially, the conversion of ethane and selectivity of ethylene were chosen as the objectives, so that a nondominated set of solutions could be obtained from a multiobjective optimization. Subsequently, other objectives were considered.

Accordingly, the optimization problem was formulated to maximize

$$J_1 = X \tag{6}$$

and

$$J_2 = S_{C_2H_4} \tag{7}$$

The variables, which prominently affect the reactor performance and can be adjusted in an industrial reactor system, were chosen as the decision variables. In the sensitivity analysis section, the effects of these variables on the objectives are discussed in detail. Following are the decision variables and the ranges used

$$700 \leq T_{in} \leq 1100 \text{ K} \tag{8}$$

$$290 \leq P_{in} \leq 500 \text{ kPa} \tag{9}$$

$$50 \leq \alpha \leq 100 \text{ kW/m}^2 \tag{10}$$

$$-100 \leq \beta \leq 0 \text{ kW/m}^2 \tag{11}$$

$$0 \leq \gamma \leq 50 \text{ kW/m}^2 \tag{12}$$

$$0.3 \leq SR \leq 0.5 \tag{13}$$

$$0.01 \leq F_{in} \leq 0.025 \text{ kmol/s} \tag{14}$$

$$n_{tubes} = 8, 9, 10, ..., 15 \tag{15}$$

$$d_{in} = 0.0953, 0.0991, 0.1080, \text{ and } 0.1143 \text{ m} \tag{16}$$

Among the decision variables, the first seven are continuous, whereas the last two (number of tubes and tube inner diameter) are discrete. For representation of the former, real coding option in NSGA-II was used, whereas for the two discrete variables, binary coding option with 3- and 2-bit sizes, respectively, was employed.

Bounds on the inlet temperature were selected according to industrial practice. A low inlet temperature indicates inefficiency in the convection section of the firebox, leaving the heating of reactants to reaction temperature to the radiation section. On the other hand, a high inlet temperature can result the designed reaction temperature in the radiation section being exceeded causing failure of the radiant coils. The upper limit on pressure depends on the upper limit on temperature and the degree of degradation of the cracking pattern caused by increasing pressure.[3] A higher pressure tends to decrease the yield of ethylene and also increases the rate of coking, both of which are undesirable. The lower bound, on the other hand, is limited by the suction pressure of the cracked-gas compressor after the quenching section, which should not fall below atmospheric pressure to avoid any oxygen in-leak.[3] Bounds on the heat-flux parameters (in eq A13) were chosen to allow maximum flexibility in the heat-flux profile. α is basically the heat flux at the beginning of the coil, and its limits were determined by the usual range of heat flux in a firebox, which is 54−96 kW/m^2,[7] whereas the bounds on β were chosen to complement α, and the bounds on γ were chosen to complement β. The values of β and γ were chosen to form a monotonically decreasing function. For the steam-to-ethane ratio (SR) and the ethane feed flow rate, the industrially employed values were used as the means for their ranges.

A typical ethylene reactor is formed of several straight tubes connected in series with suitable bends to form a long coil. In the present study, one tube in n_{tubes} includes a straight portion and a bend to facilitate a realistic enhancement of the reactor length. The length of each such tube (including bend) was taken as 9.5 m, and the number of tubes was varied from 8 to 15 in the optimization. The reactor length was thus varied from 76.0 to 142.5 m in steps of 9.5 m. The inside diameter was also varied discretely as only tubes of specific diameters are commercially available. In the present study, diameters of 0.0953, 0.0991, 0.1080, and 0.1143 m were taken as the options. Limiting values of both the number and the diameter of tubes were framed following industrial practice.[7]

Realistic constraints should be included in any optimization study. The following constraints were used in the present study

$$T \leq 1300 \text{ K} \tag{17}$$

$$P \geq 120 \text{ kPa} \tag{18}$$

$$2\gamma \leq -\beta \tag{19}$$

$$q \geq 40 \text{ kW/m}^2 \tag{20}$$

The constraints were formulated in accordance with

industrial practice. The upper limit of the reaction temperature is bound by the metallurgy of the radiant coil, which is designed to operate at 1250−1300 K when internally clean. If the temperature exceeds 1300 K, the coil can rupture without warning, so the upper limit of temperature at any point along the reactor length was fixed at 1300 K. The outlet pressure constraint was guided by the suction pressure of the cracked-gas compressor. Because the cracked gas has to go through a transfer line exchanger (TLE) for quenching after coming out of the reactor, which involves an additional pressure drop, the outlet pressure of the reactor was limited to 120 kPa. As mentioned earlier, the heat-flux profile is closely linked to the rate of coking, and the profile should be a decreasing function so that the heat input does not increase near the end of the coil and accelerate coking. The relation between β and γ in eq 19 ensures a heat flux that decreases with length. The bound on the lowest heat flux to the radiant coil (eq 20) was made to generate a realistic heat flux in the radiation section. The NSGA-II algorithm used in the present study employs a tournament-selection-based constrained nondominated sorting method for handling constraints.

Input Data for NSGA-II. The selected optimization routine, NSGA-II, for the multiobjective optimization is based on solving a minimization problem. Because the present purpose was to maximize the objective functions, the maximization problem was transformed to a minimization one as follows

$$I_1 = 1/(J_1 + 1) \qquad (21)$$

and

$$I_2 = 1/(J_2 + 1) \qquad (22)$$

The constraints were normalized as well, to keep the constraint violations within the range $[-1, 0]$, for a fairer comparison of constraint violations for the individual objectives. The normalized constraints are as follows

$$1.0 - \frac{T}{1300} \geq 0 \qquad (23)$$

$$\frac{P}{120} - 1.0 \geq 0 \qquad (24)$$

$$-\frac{\beta}{2\gamma} - 1.0 \geq 0 \qquad (25)$$

$$\frac{q}{40} - 1.0 \geq 0 \qquad (26)$$

As with many optimization methods, NSGA-II requires a set of parameters to carry out the optimization. A seed for random number generations (R_s) is required, as NSGA-II is a stochastic process. A crossover probability (p_c) and a mutation probability (p_m or $p_{m,b}$), which determine whether the crossover and mutation operation will be performed, are two other parameters that have to be supplied. The real-coded NSGA-II requires two more parameters, the distribution index for the simulated crossover operation (η_c) and the distribution index for the simulated mutation operation (η_m). Both of these values are used to define probability distributions, which ultimately determine the location of the
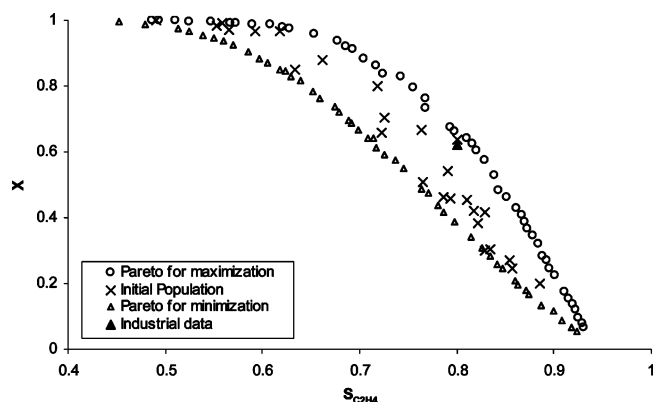

Figure 3. Pareto-optimal set obtained from the simultaneous maximization of ethylene selectivity and ethane conversion. Only the feasible points of the initial population are plotted. Also included is the Pareto of simultaneous minimization of selectivity and conversion, which represents the lower boundary of the feasible selectivity−conversion points. Industrial data point is shown by ▲.

resulting or child solution with respect to the parent solutions. Detailed descriptions of all of these parameters and real-coded NSGA-II are available in ref 25. All optimization studies were carried out with a population size of 50 and for 200 generations. The average computational time taken for each study was 3 h and 40 min, on a 2.4-GHz P4 computer with 512 MB of SDRAM.

4. Results and Discussion

In the preceding section, the objectives, decision variables, and constraints used in the optimization study were discussed in detail. In the current section, the results generated from the study are presented along with a critical analysis of the same. The objective and decision variable values were plotted suitably and were compared with the corresponding industrial data predicted by providing the industrial design and operating conditions (Table A2) to the same simulation program as was used for optimization. The predicted data, although different from the measured data, were used for comparing optimal solutions to avoid any bias arising from model limitations. The primary outcome of multiobjective optimization is the Pareto-optimal set of solutions depicting tradeoffs between the competing objectives. In addition, values of the decision variables and the trends of variation of these variables with respect to the objectives are important as well. For each multiobjective optimization study, Paretos were generated with different initial populations and various combinations of the NSGA-II parameters. The best results obtained from these studies are presented and discussed in this section.

Maximizing Ethane Conversion and Ethylene Selectivity. The Pareto-optimal set obtained by maximizing the ethane conversion and the ethylene selectivity is presented in Figure 3, which shows that the Pareto set generated by NSGA-II was smooth and well distributed over a wide range. Of the solutions in the initial population, 24 were infeasible, but the constrained nondominated sorting method brought the entire population into the feasible region by the fourth generation. Figure 3 shows only the feasible solutions of the initial population. It can be noted that the feasible solutions are not far from the final Pareto set, from the initial
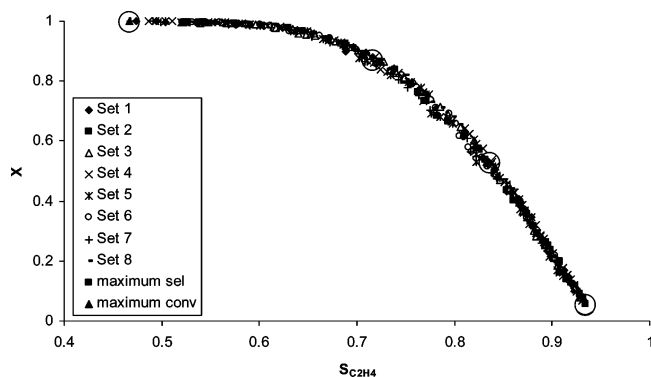
Figure 4. Pareto-optimal fronts obtained from the simultaneous maximization of ethane conversion and ethylene selectivity, obtained with different combinations of NSGA-II parameters. The parameters for sets 1–8 are listed in Table 1. Also included is the result obtained from single-objective optimizations of maximizing selectivity (■) and maximizing conversion (▲). Two additional single-objective optimization results, obtained from the ϵ-constraint method, are also plotted and shown as ×, marked by circles.

Table 1. NSGA-II Parameters Used in Figure 4

set	no. of generations	population size	p_c	p_m	η_c	η_m	R_s
1	200	50	0.85	0.05	10	20	0.6
2	200	50	0.55	0.05	10	20	0.6
3	200	50	0.95	0.05	10	20	0.6
4	200	50	0.85	0.05	10	20	0.41
5	200	50	0.85	0.01	10	20	0.6
6	200	50	0.85	0.12	10	20	0.6
7	200	50	0.85	0.05	25	20	0.6
8	200	50	0.85	0.05	10	30	0.6

population itself. This is because of the starkly contradictory nature of the objectives, for which simultaneous decreasing of both objectives is not possible below a certain limit. This limit, the Pareto of simultaneous minimization of selectivity and conversion, is also presented in Figure 3. The final Pareto set found by maximizing the objectives was identified as early as the 165th generation, after which only minor variations were noted.

The Pareto presented in Figure 3 was the best-obtained from experimentation with different combinations of NSGA-II parameters. The Paretos obtained from all of these studies ultimately reached the same front, albeit with minor variations mainly in Pareto ranges. Some of these Paretos are plotted in Figure 4, and the parameters of NSGA-II used for generating them are listed in Table 1. To further verify the fidelity of these Pareto fronts, the conversion and selectivity were optimized individually. The maximum selectivity and conversion obtained from these single-objective optimization studies perfectly lie on the two extremes of the Pareto fronts (Figure 4). An ϵ-constraint method was also applied to verify the true extent of the Pareto between the extreme values of conversion and selectivity. It was done by considering one of the objectives as a constraint and putting a lower bound on its value while maximizing the other. The study with ϵ-constraint method was carried out with both objectives, and the obtained solutions were found to be perfectly lying on the Paretos obtained by NSGA-II (Figure 4).

Among the Paretos in Figure 4, the one representing set 5 was found to be the widest and was plotted in Figure 3. It shows that, whereas the maximum ethane conversion had reached very close to 1.0, the maximum
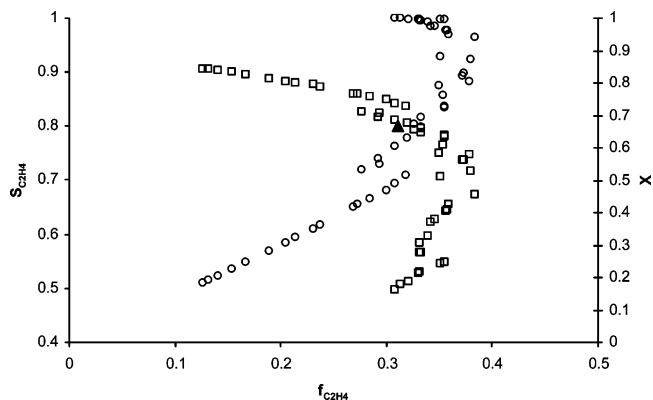

Figure 5. Ethylene flow rate versus ethylene selectivity (□) and ethylene flow rate versus ethane conversion (○) obtained from the simultaneous maximization of ethane conversion and ethylene selectivity. Ethylene flow rate versus selectivity of the industrial point is shown by ▲.

achievable selectivity was about 0.93. It can also be observed in Figure 3 that, whereas high conversion was achieved with moderate sacrifice in selectivity, achieving high selectivity needed a much higher sacrifice in conversion. For a continuous process, the unreacted ethane can be separated and recycled back, but if ethane is converted to any undesirable product, a loss is incurred. Thus, lower conversion is perhaps more acceptable than lower selectivity. On the other hand, if the process can be designed to recover side products, such as propylene and butadiene, that are higher-value products, even high conversion might become a profitable option. The best operating point can thus be determined after additional information, viz., the value of byproducts, the capital and operating costs, the controllability of the process variables, the results of hazard and safety analyses, etc., is made available and analyzed in a comprehensive way. The Pareto (Figure 3), however, brought out the intended outcome of multiobjective optimization, i.e., a wide range of competing options for design and/or operation.

The industrial point seems to represent a good tradeoff between selectivity and conversion, as the extreme objective values are avoided (Figure 3). Although it is close to the Pareto, some improvement is still possible with respect to ethane conversion and/or ethylene selectivity. Figure 5 represents the selectivity vs conversion Pareto of Figure 3 by plotting the selectivity and conversion values against the ethylene flow rate. The ethylene flow rate versus selectivity of the industrial point is also shown in the same plot. It can be seen in the figure that ethylene flow rates higher than the industrial value can be achieved with a negligible sacrifice of selectivity. Ethylene production is the primary source of profit, and if higher ethylene flow rates can be generated without affecting the selectivity or requiring a markedly different ethane flow rate, the results in Figures 3 and 5 are likely to provide better solutions than the industrial one.

Whereas the Pareto portrayed the competing nature of the objectives, the decision variables can be plotted against selectivity (Figure 6) to quantify their role in realizing the objective values. Moreover, they can be used to establish the fidelity of the optimization results as well. Figure 6a shows a clear decrease in the inlet temperature of the ethane–steam mixture with increasing selectivity, a behavior that was expected in light of the sensitivity analysis results. The inlet pressure also
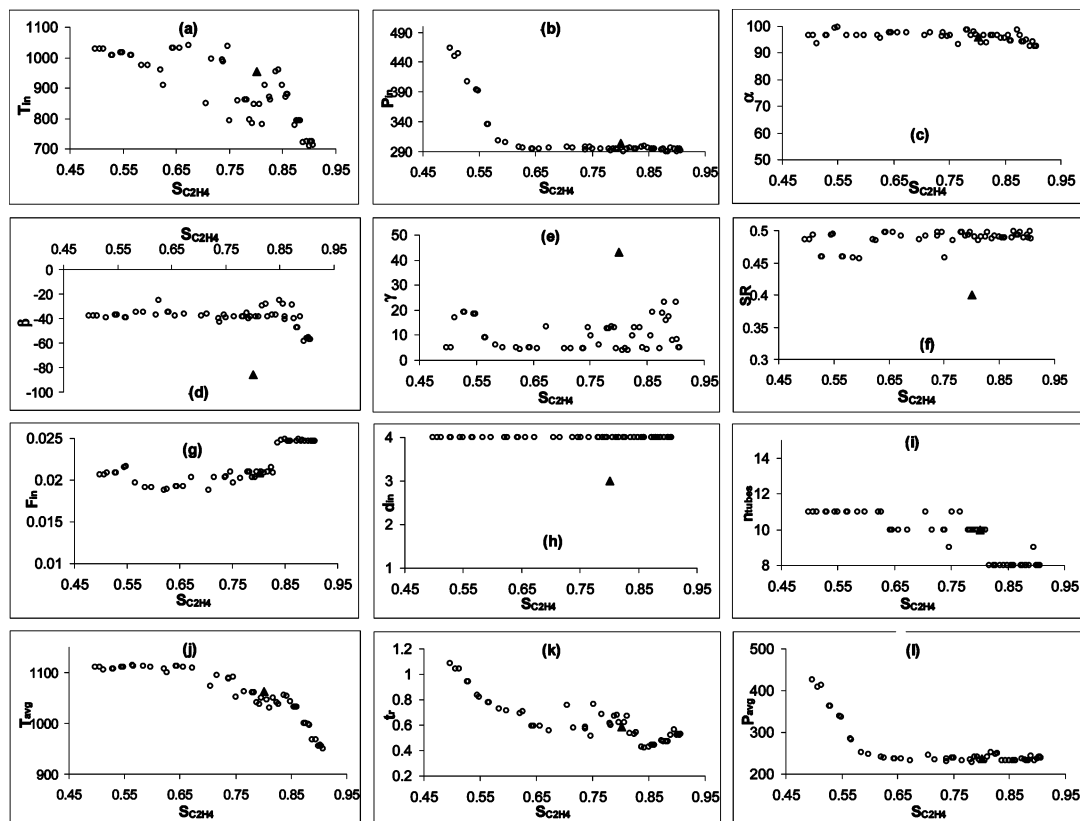
Figure 6. Decision variables and other calculated variables corresponding to the Pareto in Figure 3. Industrial data point is shown by ▲.

has high values at lower selectivity and higher conversion. However, the sharp decrease and subsequent constant values (Figure 6b), from a selectivity of 0.6 onward, suggest that the pressure facilitates the two objectives equally. The high-pressure values toward very high conversions were probably chosen to increase the residence time and, as a result, the conversion. Among the coefficients of the heat-flux function, values of α were selected very close to the upper limit (Figure 6c), whereas β and γ (Figure 6d and e) were chosen to generate a high heat flux but obey the constraint on the β and γ relation (eq 25). Values of α, β, and γ were such that heat flux was maintained high and nearly constant; the inlet temperature, on the other hand, varied to generate the Pareto. The values chosen for SR were mostly toward its upper limit (Figure 6f) to boost higher selectivity. The nature of the variation of the inlet ethane flow rate (Figure 6g) complies with the findings in the sensitivity analysis section, with relatively lower values for high conversion and higher values for high selectivity. Regarding the reactor dimensions, Figure 6h shows that the largest available reactor diameter was chosen uniformly for the entire Pareto. Note that the discrete values used in the optimization study for reactor inside diameters were replaced by numbers 1−4 in ascending order in the plot of the diameter values in Figure 6h and in all other subsequent cases. The number of reactor tubes (Figure 6i), on the other hand, decreased to reduce the residence time, thus facilitating the selectivity increment.

A comparison of the industrial design and operating conditions with those obtained by the optimization study reveals that, whereas the inlet pressure, ethane flow rate, and number of tubes used in the reactor were similar in the two cases, the values of the other decision variables varied widely. The inlet temperature values

are often far lower than their industrial counterpart (Figure 6a). Whereas the α values are similar in the two cases, the β and γ values differ widely, forming very different heat-flux profiles for the two cases. The average reaction temperature (Figure 6j), however, shows that the industrial reactor operates at a slightly higher temperature. As lower-temperature operation is more desirable from material- and energy-savings points of view, the decision variable values suggested by the optimization seem to be better. The steam-to-ethane ratio (SR) used in industry is lower than the study-generated values. A lower SR value is more desirable as it reduces the volume of material handling and affects all related costs. The reactor diameter, on the other hand, was chosen larger than the industry value. A larger reactor diameter, although it increases the residence time and facilitates conversion, involves a higher capital investment.

The decision variable values in Figure 6, although having clear trends, are relatively scattered in nature when compared to the smooth variation of the Pareto set they generated (Figure 3). There are two plausible causes for this scattering: first, the objective functions are weakly dependent on the decision variable(s), so that even a considerable variation in decision variable values did not affect the former significantly, and second, more than one combination of multiple decision variables had similar effects on one or more of the objective values. During the sensitivity analysis, it was found that all of the decision variables have a strong influence on at least one of the objectives; this refutes the plausibility of the first cause. However, to investigate further, decision variables corresponding to the Paretos of sets 1, 3, and 6 (Figure 4) were plotted simultaneously in Figure 7. It can be seen in this figure that, although their respective Pareto-optimal fronts coincide, the corresponding deci-
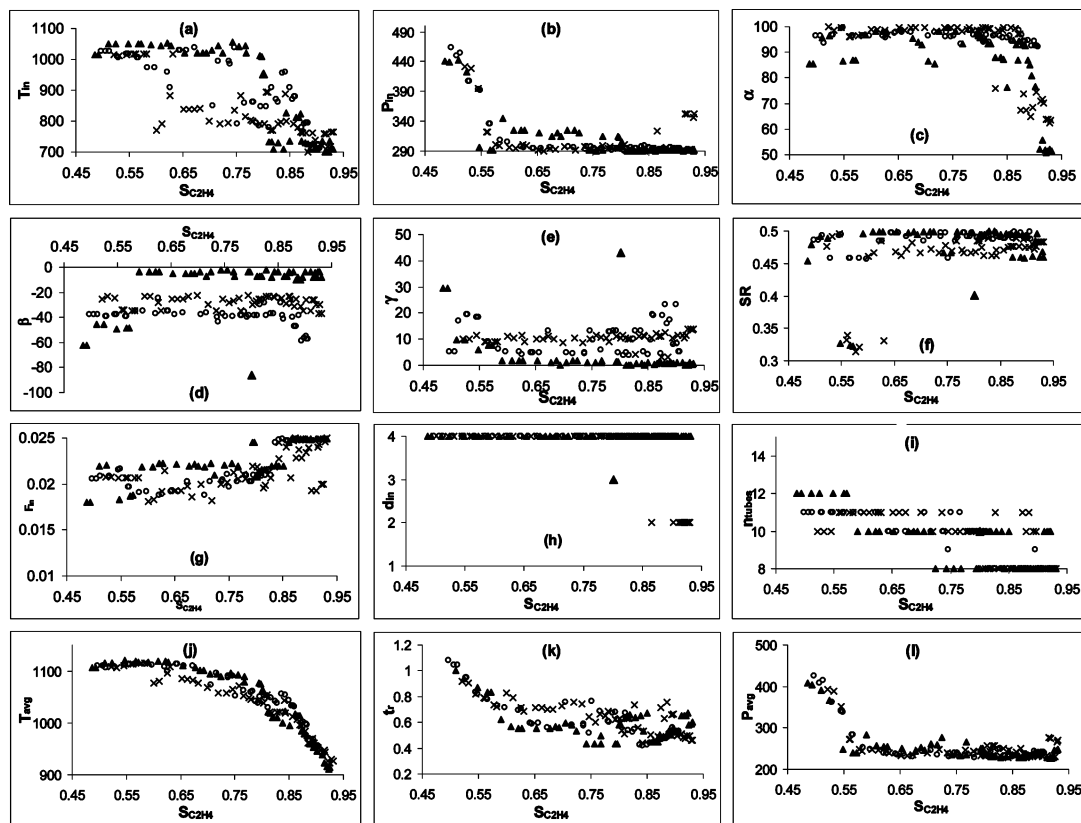
Figure 7. Decision variables and other calculated variables corresponding to the three Paretos of Figure 4 represented by set 1 (○), set 3 (▲), and set 6 (×) of Table 1.

sion variables are different from one another. The most noticeable variations are in the values of inlet temperature (T_{in}) (Figure 7a); β (Figure 7d); γ (Figure 7e); ethane flow rate (F_{in}) (Figure 7g); and to some extent, number of reactor tubes (n_{tubes}) (Figure 7i), all of which have significant individual influences on the objectives (Figure 2). Interestingly, for all three sets, values of the average temperature (Figure 7j), which is strongly dependent on the values of T_{in}, β, and γ, show similar trends with very close values. In fact, values of all of the main controlling variables, i.e., average temperature (T_{avg}), residence time (t_r), and average pressure (P_{avg}), show clearer trends compared to the scattered values of the decision variables (Figure 7j−l); whatever minor scattering is observed can be attributed to their compensatory effects on one another. In other words, different combinations of these three variables can produce very similar conversion and selectivity values. For example, a lower residence time can be compensated by a high average temperature or a high average pressure, to result in the same conversion. The scattering in the values of the decision variables (Figure 6a−i, on the other hand, are much wider because the degrees of freedom of the decision variables are more than those of the controlling variables.

For further verification, we carried out a series of multiobjective optimization studies with different numbers and different sets of decision variables, the results of which are presented in Figures 8 and 9. In all of these studies, decision variables that are not varied take the industrial reactor values, except for the inlet pressure and ethane flow rate, which were taken as 350 kPa and 0.025 kmol/s, respectively. It was observed that, with inlet temperature as the only decision variable, there was no scattering of either the Pareto or the decision

variable values (Figures 8 and 9a), even when the study was carried out with four different combinations of NSGA-II parameters and initial populations. The Pareto formed by this study, however, was short (Figure 8) compared to the original Pareto (Figure 3), producing high selectivity values and conversion values lower than 65%. Similar results were obtained from the studies with inlet temperature and inlet pressure as the decision variables (Figures 8, 9b, and 9c), although there was slight improvement of the Pareto (Figure 8), but that was not significant compared to the Pareto of Figure 3. It can be noted in Figure 9b and c that, even with the highest available temperature and pressure, the conversion could not be taken above 70% (Figure 8). Even introduction of α as the third decision variable could not improve the Pareto (Figure 8), even though mild scattering in the decision variable values was registered (Figure 9d−f). Adding reactor inside diameter as the fourth decision variable could improve the Pareto, taking the conversion up to 82% (Figure 8), although it caused more scattering (Figure 9g−i) in the decision variables. The selected reactor diameter was generally the highest available option (Figure 9i).

The trends of the decision variables as seen up to Figure 9i provide a clear hint that, unless the reactor volume is increased sufficiently, even the highest temperature and pressure cannot take the conversion higher. To implement this change, the number of reactor tubes was added as the fourth decision variable, replacing the diameter. This was done because n_{tubes} had more volume increment options. It can be seen in Figure 8 that using n_{tubes} as a decision variable could generate a broader Pareto and took the conversion up to 100%. The decision variables, however, are scattered (Figure 9j−l). To see the potential of T_{in} and n_{tubes} as decision
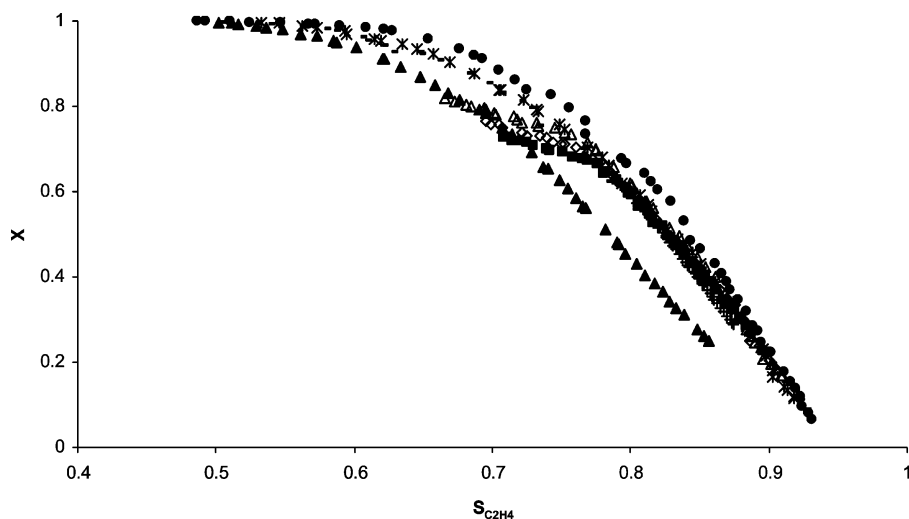
Figure 8. Pareto-optimal fronts formed by (●) nine decision variables, (+) one decision variable (T_{in}), (■) two decision variables (T_{in} and P_{in}), (▲) two decision variables (T_{in} and n_{tubes}), (◇) three decision variables (T_{in}, P_{in}, and α), (△) four decision variables (T_{in}, P_{in}, α, and d_{in}), (—) four decision variables (T_{in}, P_{in}, α, and n_{tubes}), and (*) five decision variables (T_{in}, P_{in}, α, d_{in}, and n_{tubes}).

variables, a two-variable optimization study was carried out with them. The results (Figure 9m−o) show that they could take the conversion very close to 100%, but the Pareto generated was far inferior to the original Pareto (Figure 8). The main reason for this difference, as understood, was the choice of very high value (500 kPa) for the fixed inlet pressure of the study. High pressure was chosen to allow the optimizer to select a higher number of reactor tubes, and thus increase the reactor volume, without getting rejected by the pressure constraint (eq 18). This study brought out a clearer picture regarding the individual contributions of T_{in}, n_{tubes}, and P_{in} in generating selectivity−coversion Paretos. When a five-variable study was carried out, including diameter with the previous set, no significant difference was observed in the Pareto or the trends of the decision variables (Figure 8). It can be concluded from this study that, when sufficient volume increment option, are provided to the optimizer along with high temperature and pressure options, scattering in decision variable values is sure to creep in. This is because a high reactor volume can easily compensate lower reaction temperature to achieve high conversion and vice versa, so different combinations of reactor volumes and reaction temperatures (which themselves result from multiple combinations of T_{in}, α, β, and γ) can achieve the same result.

The above analysis clearly shows that the scattering in decision variable values is due to the high number of degrees of freedom in the studied problem. It also indicates that, after the Pareto-optimal set is identified, a systematic approach to finding the most desirable sets of decision variables to realize these optimal points should be devised. This might dramatically change the acceptability of suggestions regarding optimal design and operating conditions by offering more feasible and achievable choices to the designers and plant operators. In a recent work, Deb[30] demonstrated the importance of such studies with decision variables for innovative designs.

During the simultaneous maximization of ethane conversion and ethylene selectivity, it was noticed that the highest ethylene flow rate obtained by the study was generated by an ethane flow rate far lower than its highest possible value. On the other hand, high ethane flow rates close to the upper limit were chosen to maximize selectivity, but they also resulted in lower ethylene flow rate values. It was concluded from these two observations that an exclusive criterion should be included in the optimization process that will ensure the production of the highest possible ethylene flow rate. To this end, two more two-objective optimization studies, of maximizing (1) the ethylene flow rate and selectivity and (2) the ethylene flow rate and the ethane conversion, were performed. These studies generated many possible design options, offering a higher number of choices for the best-suited combination. In addition, the prospect of a higher ethylene flow rate is attractive because it influences the profitability significantly.

Maximizing Ethylene Flow Rate and Selectivity. The results of maximizing ethylene flow rate and selectivity simultaneously are presented in Figures 10−12. In the initial population, there were 24 infeasible solutions, and as in the previous study, all the solutions were brought into feasible region by the fourth generation. By the 175th generation, the final Pareto was reached, after which the solutions varied insignificantly until the last generation. The Pareto was obtained with set 1 parameters (Table 1) of NSGA-II. Figure 10 shows only the feasible points of the initial population.

It can be seen from the Pareto (Figure 10) that the highest ethylene flow rate achieved was 20% greater than that obtained by maximizing ethane conversion and ethylene selectivity (Figure 5). When selectivity versus conversion values obtained from (i) maximizing the ethane conversion and ethylene selectivity and (ii) maximizing the ethylene flow rate and selectivity were compared (Figure 11), it was observed that the two sets of results coincided except that the ranges were different. At first glance, the Pareto in Figure 10 seems to offer better operating points with higher ethylene selectivities and flow rates than the industrial data. This picture, however, is not completely true. Figure 11 shows that the industrial point is very close to the selectivity versus conversion Pareto. In the Pareto of Figure 10, a higher ethylene flow rate is achieved at a selectivity equal to the industrial point, because of the use of about 20% higher ethane flow rate (Figure 12g).

Some trends in the plots of decision variables against ethylene flow rate (Figure 12) corresponding to the Pareto in Figure 10 are similar to those in Figure 7. The inlet temperature of the ethane−steam mixture
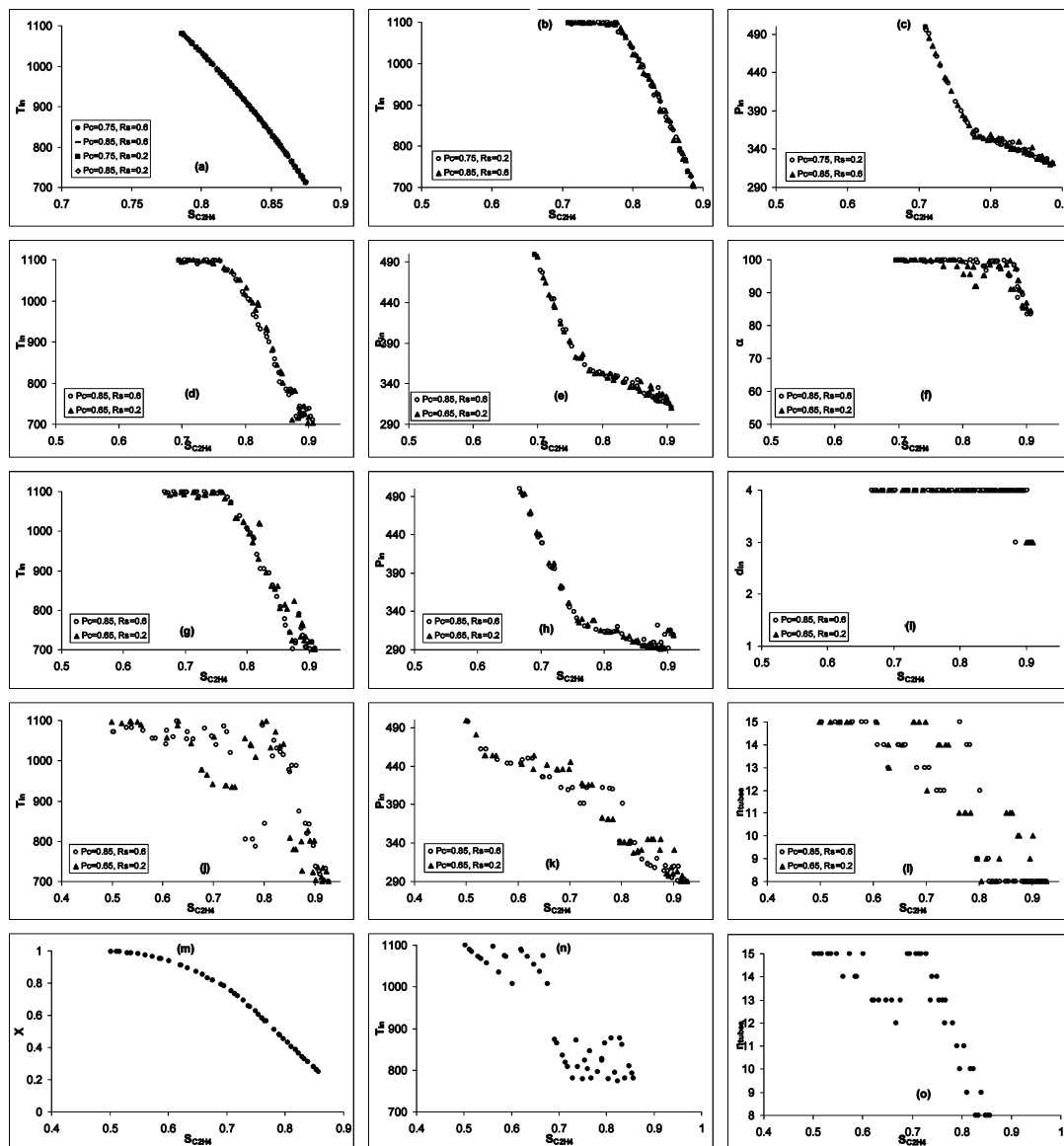
Figure 9. (a) Decision variables (T_{in}) of 1-variable study, (b & c) decision variables (T_{in} and P_{in}) of 2-variable study, (d, e & f) decision variables (T_{in}, P_{in}, & α) of 3-variable study, (g, h & i) three of the decision variables (T_{in}, P_{in}, d_{in}, and α) of 4-variable study, (j, k & l) three of the decision variables (T_{in}, P_{in}, n_{tubes}, and α) of another 4-variable study, (m, n & o) Pareto and decision variables (T_{in} & n_{tubes}) of another 2-variable study.
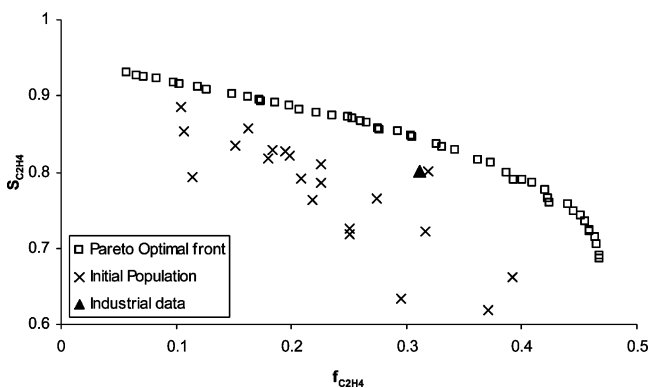

Figure 10. Pareto-optimal set obtained from the simultaneous maximization of ethylene flow rate and selectivity. Only the feasible points of the initial population are plotted. Industrial data point is shown by ▲.
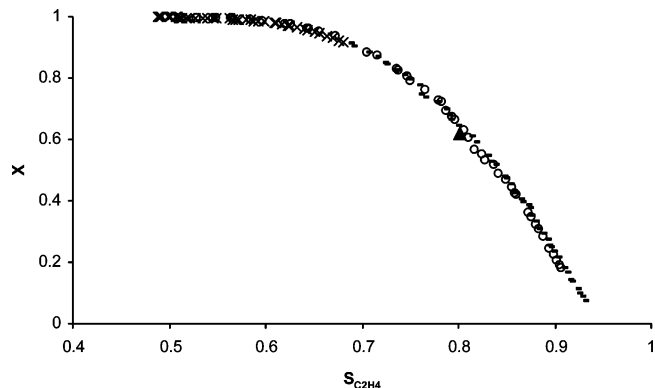

Figure 11. Comparison of the conversion versus selectivity obtained by (a, ○) maximizing ethane conversion and ethylene selectivity, (b, —) maximizing ethylene flow rate and selectivity, and (c, ×) maximizing ethylene flow rate and ethane conversion. Industrial data point is shown by ▲.

rose first moderately (Figure 12a) and then abruptly at ethylene flow rates above 0.3 kg/s. On the other hand, α exhibited a reverse trend (Figure 12c): it steadily

increased to its upper limit and stayed almost invariant there. This shows that the optimizer initially increased the heat flux to its upper limit and then increased the
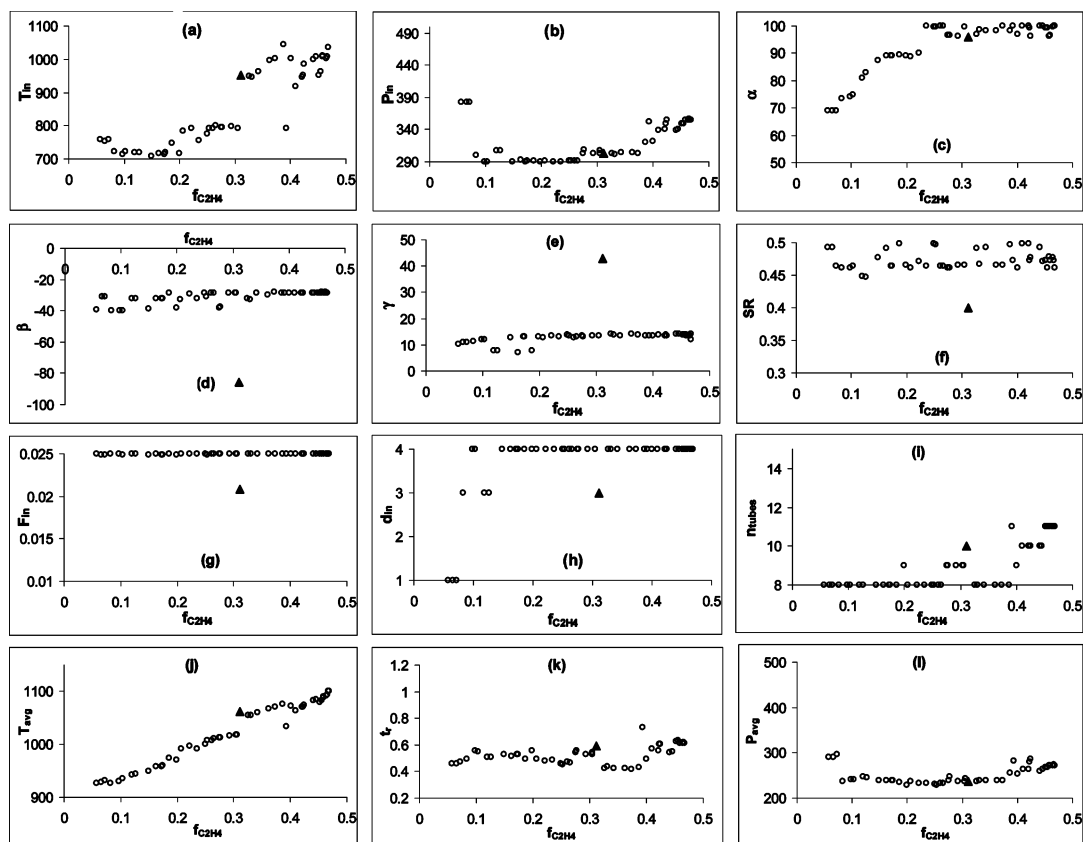
Figure 12. Decision variables and other calculated variables corresponding to the Pareto in Figure 10. Industrial data point is shown by ▲.

inlet temperature to steadily increase the reaction temperature. The steady increase of the average reaction temperature supports this analysis (Figure 12j). Values of β and γ (Figure 12d and e), however, stayed almost invariant throughout the Pareto range. The inlet pressure of the ethane−steam mixture was mostly chosen near the lower bound to keep the selectivity high; however, toward higher ethylene flow rates, the inlet pressure increased to boost the conversion by increasing the residence time (Figure 12b and k). The occurrence of a few high-inlet-pressure points at the lower ethylene flow rates is probably because of the smaller tube diameter chosen (Figure 12h). The SR value, on the other hand, was selected toward the upper bound to enhance selectivity (Figure 12f); the slight scatter in its values is due to its marginal effect on the objectives. The ethane flow rate was chosen throughout very close to the upper bound (Figure 12g), probably to maximize the ethylene flow rate, which is one of the objectives.

Optimal reactor dimensions were also consistently chosen: reactor diameter is generally the largest available value, and number of tubes is the lowest (Figure 12h and i). The latter takes slightly higher values at higher ethylene flow rates, probably to increase the residence time and conversion. The pressure rise toward higher ethylene flow in Figure 12b might be due to the increasing reactor length. A close comparison of residence time (Figure 12k), reactor length (Figure 12i), and inlet pressure (Figure 12b) reveals their interdependence. Whereas the pressure and residence time values did not vary significantly throughout most of the ethylene flow rate range, the Pareto between ethylene selectivity and flow rate was mainly influenced by the monotonically rising average reaction temperature (Figure 12j). Although industrial data are similar to the
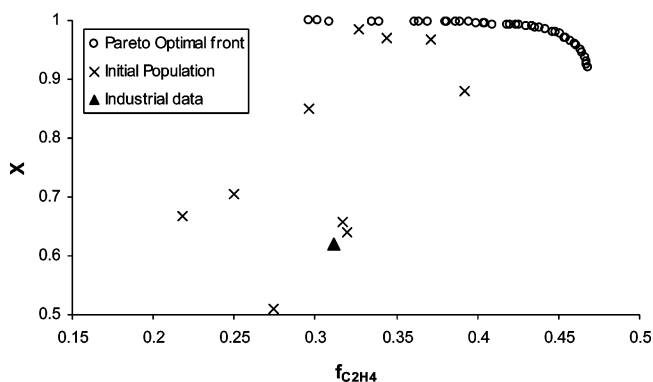

Figure 13. Pareto-optimal set obtained from the simultaneous maximization of ethylene flow rate and ethane conversion. Only the feasible points of the initial population are plotted. Industrial data point is shown by ▲.

optimal values obtained for inlet pressure, α, number of tubes, residence time, and average reaction pressure, they differ in the other decision variables found by multiobjective optimization (Figure 12). Average reaction temperature is slightly higher for the industrial data (Figure 12j) because of the higher values of inlet temperature, β, and γ (Figures 12a, d, and e). SR, ethane flow rate, and tube diameter in the industrial data are much lower than those found by optimization (Figure 12f−h).

Maximizing Ethylene Flow Rate and Ethane Conversion. The Pareto-optimal set obtained by maximizing the ethylene flow rate and ethane conversion is presented in Figure 13. The initial population had 32 infeasible solutions, all of which were guided to the feasible zone by the fourth generation. The final Pareto was reached by 110th generation, after which insignifi-
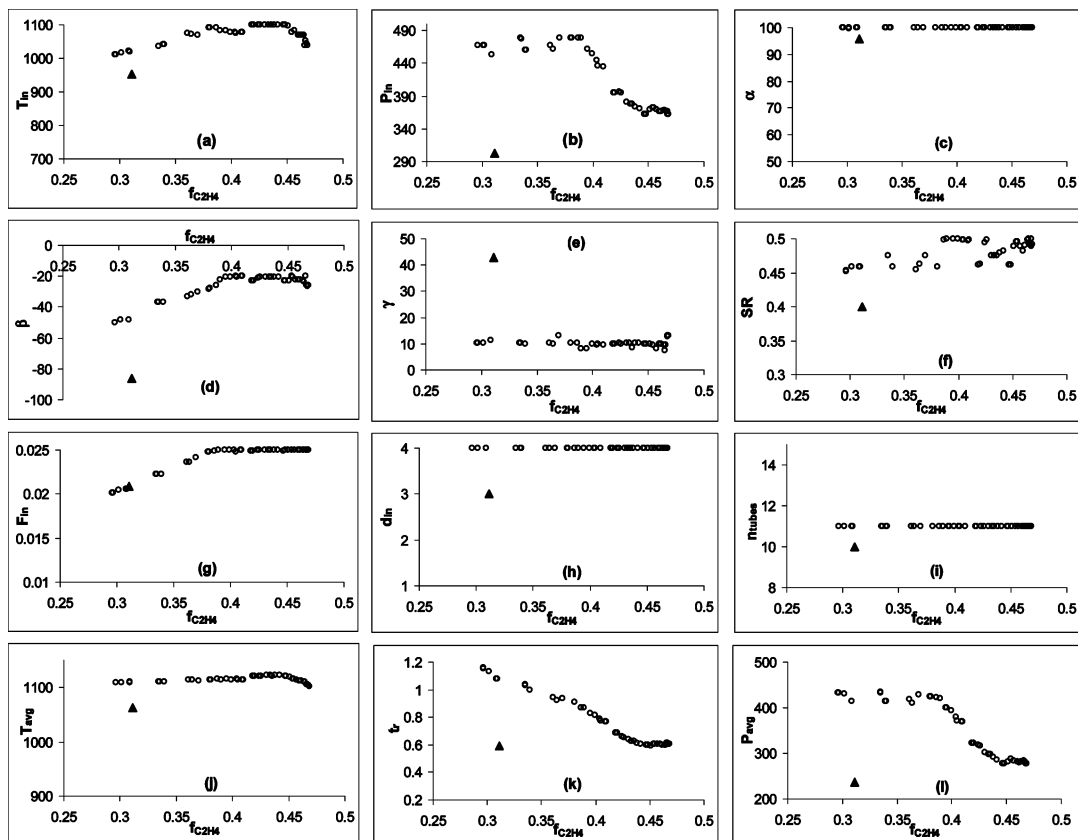
Figure 14. Decision variables and other calculated variables corresponding to the Pareto in Figure 13. Industrial data point is shown by ▲.

cant variations were noted. Set 1 parameters (Table 1) of NSGA-II were used for generating this Pareto.

It can be observed that the ethylene flow rate−ethane conversion optimization process generated high conversions, varying from 92 to 100% (Figure 13), where the ethylene flow rate varied from 0.47 to 0.3 kg/s. The latter is less than that (varied from 0.05 to 0.47 kg/s in Figure 10) found by maximizing the ethylene flow rate and selectivity. Interestingly, the selectivity and conversion values corresponding to the Pareto in Figure 13 complement those obtained by maximizing the ethylene flow rate and selectivity (Figure 11), and the two sets, together, coincide with the selectivity−conversion Pareto in Figure 3. This shows that two separate two-objective optimization studies, involving optimization of the pairs flow rate−selectivity and flow rate−conversion, together, can generate a selectivity−conversion plot very similar to the Pareto found by maximizing selectivity−conversion. The range of the combined curve, however, is greater than that of the latter, and even the population is better distributed. None of the optimal solutions from the maximization of the ethylene flow rate and ethane conversion (Figure 13), however, would be attractive because of their low selectivity values.

The values of the decision variables, when plotted against the ethylene flow rate (Figure 14a−i), varied quite differently as compared to their variations in the previous two studies. The inlet temperature gradually rose from 1000 K to the maximum value and then decreased toward higher ethylene flow rates (Figure 14a). Although α was at its upper bound and γ was closer to its lower bound for the entire Pareto (Figure 14c and e), the variation of β was similar to that of the inlet temperature (Figures 14a and d). The variation of

the average reaction temperature (Figure 14j) is similar to that of the inlet temperature and β. The inlet pressure was very high at lower ethylene flow rates to provide larger residence times to maximize the ethane conversion (Figure 14b). SR (Figure 14f) is generally high with some scatter. Low values of the ethane flow rate were chosen initially (Figure 14g) to increase the residence time and conversion (Figure 14k), but the ethane flow rate was increased toward higher ethylene flow rates. The reactor dimensions chosen in this study were invariant (Figures 14h and i) and the highest possible values satisfying the constraints and bounds. This was to create the maximum possible residence time to ensure maximum possible conversion. The residence time (Figure 14k) was initially high at about 1.2 s because of the high inlet pressure coupled with the low ethane flow rate; it gradually decreased with increasing ethylene flow rate and then became flat at ethylene flow rates above 0.45 kg/s.

A comparison between the results of maximizing the ethylene flow rate and ethane conversion and the industrial data reveals interesting differences. The average reaction temperature, residence time, and inlet pressure (Figure 14j−l) from the optimization are much higher than those in the industrial data. As can be seen in Figure 14a−i, many decision variables, including inlet temperature, inlet pressure, heat-flux function coefficients, SR, and reactor dimensions, have higher values than the industrial data. Although the ethane flow rate is close for the two cases (Figure 14g), the conversion is much higher (Figure 13). The operating conditions suggested by optimization can be useful if high conversion is desired.

Maximizing Ethylene Flow Rate, Ethylene Selectivity, and Ethane Conversion. Optimization
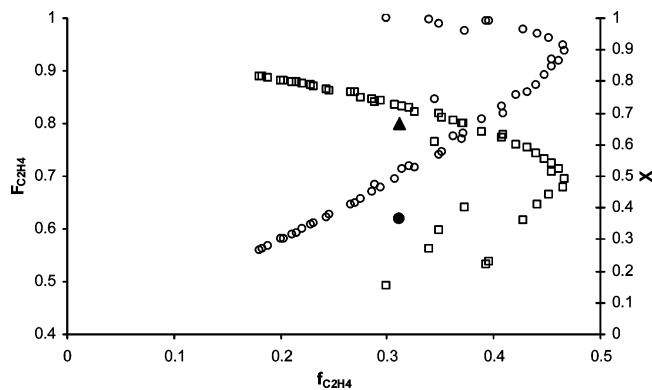
Figure 15. Pareto-optimal set obtained from the simultaneous maximization of ethylene flow rate, ethylene selectivity, and ethane conversion. (a) Ethylene flow rate vs selectivity values (○) and corresponding industrial data point (▲). (b) Ethylene flow rate vs ethane conversion values (□) and corresponding industrial data point (●).

Figure 16. Comparison between the Pareto-optimal set obtained from the three-objective optimization (●) and the selectivity–conversion two-objective optimization (○) studies. For the former case, the values of ethylene flow rate, ethylene selectivity, and ethane conversion were obtained from the optimization, whereas for the latter, the ethylene flow rate was calculated from the optimal selectivity and conversion values.

studies with ethylene flow rate as one of the objectives show the clear difference in the nature of the variations of both decision variables and objectives, as compared to the results generated by selectivity−conversion optimization study. This shows that the ethylene flow rate as an objective is not redundant in a multiobjective optimization study even though its value depends on the other two objectives. Hence, a three-objective optimization study taking all three objectives was carried out for complete analysis. Figure 15 presents the Pareto generated by maximizing ethane conversion, ethylene selectivity, and flow rate simultaneously. In this figure, selectivity and conversion are plotted against ethylene flow rate. The curves thus generated show that, even though ethylene flow rate continually increased with increasing conversion and decreasing selectivity, there was a maximum value beyond which the ethylene flow rate decreased against increasing conversion and selectivity values. The results obtained from the three-objective optimization when compared with the results from the two-objective optimization of conversion and selectivity (Figure 16) showed a high increment of ethylene flow rate for the former case, although the tradeoff between selectivity and conversion remained the same.

When the flow rate vs selectivity and flow rate vs conversion values from the latter two optimization studies were plotted in a single graph (Figure 17) with the three-objective optimization Pareto, the combined results of the two-objective optimizations were found to be very close to the three-objective optimization results. It can be noted in the overall figure, which involved plotting any combination of the three objectives used in this study, that, in some plots, the y-axis variable either increased or decreased monotonically with increasing x-axis variable, whereas in others, the y-axis variable showed both increasing and decreasing trends with increasing x-axis variable. For example, in Figure 3, which shows a plot of the tradeoff between the selectivity and conversion, conversion monotonically decreases with increasing selectivity. When the same Pareto is plotted (Figure 5) against the ethylene flow rate values, however, the changes in selectivity and conversion with respect to the flow rate are found to be nonmonotonic. This is because multiobjective optimization works only on conflicting objectives to generate nondominated points. Conversion of ethane and selectivity of ethylene are truly conflicting in nature (which
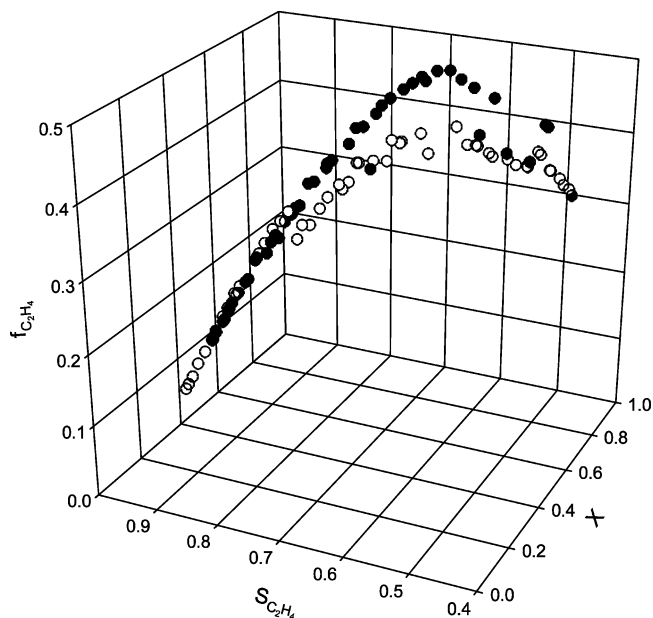
was also evident from the sensitivity analysis), so they formed a perfect Pareto of nondominated points (Figure 3) covering almost the entire range of conversion values. In Figure 5, on the other hand, the ethylene flow rate values are only *plotted* against the two objectives, it does not represent the Pareto. Thus, the plot displays both conflicting and nonconflicting relationships of ethylene flow rate with the two objectives. Similarly, Paretos generated by maximizing the ethylene flow rate with selectivity and conversion were formed just up to the end of the conflicting region. The points beyond were discarded by the optimizer because they all would have been dominated by the present Pareto points. This nature can be clearly viewed in Figure 17, where the nonconflicting portions of flow rate vs selectivity and flow rate vs conversion were obtained from the results of each other. For example, the nonconflicting points of the flow rate vs conversion plot in Figure 17 (■) were actually obtained during the flow rate vs selectivity optimization. The three-objective optimization, on the other hand, could generate both conflicting and non-conflicting points because the criterion of domination was sufficiently fulfilled by a point if any of the three objectives had a sufficiently high value, despite simultaneous devaluation of the other two objectives.

To understand the full gamut of the respective variations, decision variables from the three-objective optimization are presented in Figure 18 along with those from the flow rate−selectivity and flow rate−conversion optimizations. The figure exhibits a very interesting interrelationship of individual decision variables from different optimization studies. It can be seen that the results of two two-objective optimizations complement each other, whereas the three-objective optimization results follow partly the wider range of results obtained from maximizing flow rate−selectivity and flow rate−conversion. A discussion of the variations of decision variables in the three-objective optimization is not needed because it is similar to the previous analyses.
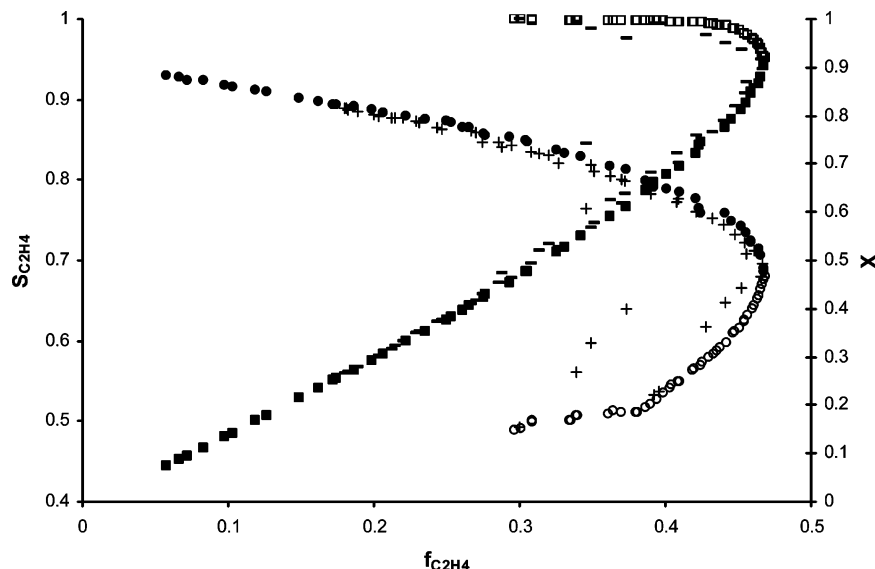
Figure 17. Comparison of (a) ethylene selectivity versus ethylene flow rate and (b) ethane conversion vs ethylene flow rate obtained from (1) ethylene flow rate−selectivity maximization (●, a; ■, b); (2) ethylene flow rate−ethane conversion maximization (○, a; □, b); and (3) three-objective optimization of ethylene flow rate, ethylene selectivity, and ethane conversion (+, a; −, b).
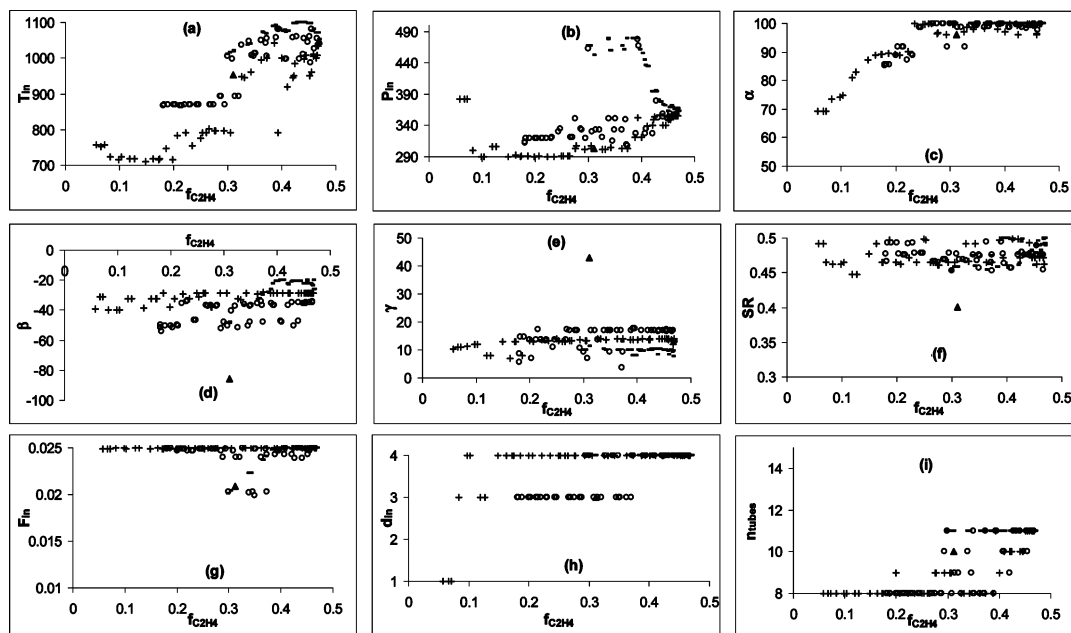

Figure 18. Combined plot of decision variables from (a, +) maximizing ethylene flow rate and selectivity; (b, −) maximizing ethylene flow rate and ethane conversion; and (c, ○) three-objective optimization of ethylene flow rate, ethylene selectivity and ethane conversion. Industrial data point is shown by ▲.

5. Conclusions

Optimization of an industrial ethylene reactor using an ethane feed for two and three objectives was successfully performed using a GA-based optimizer, NSGA-II. The reactor was modeled following a more accurate but complex free-radical scheme[8] for accurate predictions. The optimization problem involved seven continuous variables and two discrete variables as well as realistic constraints. Trends of optimal values of objectives and decision variables could be explained qualitatively, which shows the reliability of the results. In the first part of the study, ethane conversion and ethylene selectivity were chosen as objectives because they are exactly contradictory. The generated results indicated that inclusion of the ethylene flow rate as another objective was required to develop further insight into the process. Two more two-objective optimiza-

tions and a three-objective optimization study were carried out using objective combinations of flow rate−conversion, flow rate−selectivity, and flow rate−conversion−selectivity, respectively. The results showed that the two two-objective optimization studies are complementary and the combined results follow those from the three-objective optimization study. However, the combined results have a wider range, better results, and smoother variations of conversion and selectivity values against flow rate.

The study produced a wide gamut of optimal design and operational options for the ethylene reactor, revealing a qualitative as well as quantitative relation of the reaction process with the design and operation variables. It demonstrated both the individual and combined roles played by reactor temperature, reactor pressure, and residence time in achieving the objectives. It was

Table A1. Molecular Species and Free Radicals for Ethane Cracking

j	molecular species	j	free radical
1	methane, CH_4	12	$H\bullet$
2	acetylene, C_2H_2	13	$CH_3\bullet$
3	ethylene, C_2H_4	14	$C_2H_3\bullet$
4	ethane, C_2H_6	15	$C_2H_5\bullet$
5	propylene, C_3H_6	16	$C_3H_5\bullet$
6	propane, C_3H_8	17	$1\text{-}C_3H_7\bullet$
7	butadiene, C_4H_6	18	$C_4H_7\bullet$
8	1-butene, $1\text{-}C_4H_8$	19	$1\text{-}C_4H_9\bullet$
9	n-butane, $n\text{-}C_4H_{10}$	20	$C_5H_{11}\bullet$
10	$C_{5+}{}^a$		
11	hydrogen, H_2		

^{a} Taken to be 1-pentene, C_5H_{10}.

found that a larger reactor volume is necessary for higher conversion, whereas the reverse is true for higher selectivity. To vary the reactor volume, the optimizer almost always varied the number of reactor tubes while keeping the reactor inside diameter constant at the upper limit. The reasons for this result are that (a) the highest reactor diameter was selected throughout to reduce the reactor pressure drop and thus avoid any rejection of a good solution because of a violation of the outlet pressure constraint (eq 18) and (b) the optimizer had the maximum flexibility of changing the reactor volume, and thereby the residence time, by changing the reactor length. High inlet temperatures were chosen to achieve high conversions, whereas lower temperatures were chosen for high selectivity. The study showed that, although lower inlet pressure is beneficial for all of the tradeoffs, higher pressures should be chosen toward very high conversions. This is mainly to accommodate the pressure drop caused by the choice of a higher number of tubes to boost conversion.

It was observed that the most important decision variables used in this study were the reactor inlet temperature and the length of the reactor (represented by the number of reactor tubes). This is because, by manipulating the values of these two variables only, a Pareto ranging from ~100% conversion to over 85% selectivity could be produced. However, it was also observed that, unless the values of the other decision variables are properly controlled, the reactor performance cannot achieve the best conversion−selectivity tradeoffs. In other words, to achieve a particular conversion with the best compromise in selectivity (or vice versa), one has to manipulate mainly the reactor inlet temperature and the number of reactor tubes. Values of other variables can be micromanaged to reach the desired tradeoff point.

In general, a multiobjective optimization study is beneficial for understanding the performance tradeoff of conflicting objectives and decision variables and for producing a wide range of optimal solutions.

Appendix A

Molecular and free-radical species in the free-radical mechanism of ref 8 for ethane cracking are listed in Table A1. Governing equations for the steam cracker are as follows:

A.1. Material Balance. For the case of the free-radical scheme for ethane cracking, there are 20 species in total: 11 molecular species and 9 free radicals. The mass balance equation is given by

$$\frac{dF_j}{dx} = \left(\sum_i \alpha_{ij} r_i\right)\left(\frac{\pi d_{in}{}^2}{4}\right) \tag{A1}$$

with the rate of reaction, r_i, expressed as

$$r_i = k_i \prod_j C_i \tag{A2}$$

where

$$k_i = A_i \exp\frac{-E_i}{RT} \tag{A3}$$

$$C_j = \left(\frac{F_j}{F_T}\right)\left(\frac{P}{RT}\right) \tag{A4}$$

$$F_T = F_{steam} + \sum_j F_j \tag{A5}$$

for $i = 1, 2, 3, ...,$ number of reactions, and $j = 1, 2, 3, ...,$ total number of species (excluding steam).

A.2. Energy Balance. The energy balance equation was written in terms of the heat of formation for each molecular species. Free radicals, being of much smaller concentrations than molecular species, are ignored in the following differential equations

$$\frac{dT}{dx} = \frac{q(x)\pi d_{in} - \sum_j \left[(\Delta H_{f,j})\dfrac{dF_j}{dx}\right]}{\sum_j F_j C_{p,j} + F_{steam} C_{p,steam}} \tag{A6}$$

with

$$\Delta H_{f,j} = (\Delta H^\circ_{f,298})_j + \int_{298}^T C_{p,j}\, dT \tag{A7}$$

for $j = 1, 2, 3, ...,$ total number of molecular species.

A.3. Momentum Balance. The momentum balance equation was formulated to accommodate the calculation of the additional pressure drop in the bends by using a friction factor, F_r[7]

$$\frac{dP}{dx} = \frac{\dfrac{\sum_j \dfrac{dF_j}{dx}}{G_m A_t} + \dfrac{1}{M_m}\left(\dfrac{1}{T}\dfrac{dT}{dx} + F_r\right)}{\dfrac{1}{M_m P} - \dfrac{g_c P}{G_m{}^2 RT}} \tag{A8}$$

The friction factor for straight tubes given by[31]

$$F_r = 0.092\frac{Re^{-0.2}}{d_{in}} \tag{A9}$$

The friction factor for bends is given by[32]

$$F_r = 0.092\frac{Re^{-0.2}}{d_{in}} + \frac{\zeta}{\pi R_b} \tag{A10}$$

Table A2. Design and Operating Conditions for the Industrial Reactor Taken from Ref 5

parameter	value
inlet ethane−steam mixture temperature (K)	953
inlet ethane−steam mixture pressure (kPa)	303
steam-to-ethane mass ratio (SR)	0.4
inlet ethane flow rate[a] (kmol/s)	0.020 87
tube inside diameter (m)	0.108
number of straight tubes (each 8.941 m long)	10
number of bends (each 0.559 m long)	10
total reactor length (m)	95

[a] Composition: 98.2% ethane, 1% ethylene, and 0.8% propylene.

Table A3. Comparison of Predictions by the Model with the Industrial Data in Ref 5

parameter	measurement	model prediction
coil outlet temperature (K)	1108	1121
coil outlet pressure (kPa)	131.7	132.3
conversion	0.599	0.618
CH_4 exit flow rate (kmol/s)	0.00131	0.0013
C_2H_4 exit flow rate (kmol/s)	0.0109	0.011 09
C_2H_6 exit flow rate (kmol/s)	0.008 22	0.007 827
C_3H_6 exit flow rate (kmol/s)	0.000 160	0.000 137

where

$$\zeta = \left(0.7 + 0.35\frac{\Lambda}{90°}\right)\left(0.051 + 0.19\frac{d_{in}}{R_b}\right) \quad \text{(A11)}$$

and

$$Re = \frac{d_{in}G_m}{\mu_m} \quad \text{(A12)}$$

The heat-flux profile in the radiation section of the reaction system was represented by a quadratic expression that is a function of a fraction of the total length of the reactor, L

$$q(x) = \alpha + \beta\left(\frac{x}{L}\right) + \gamma\left(\frac{x}{L}\right)^2 \quad \text{(A13)}$$

where α, β, and γ are suitable coefficients. Design and operating conditions of the industrial ethylene reactor taken from ref 5 are listed in Table A2. The coefficients in eq A13 are $\alpha = 96$, $\beta = -85.91$, and $\gamma = 42.955$, all in kW/m^2, which provide a heat-flux profile matching the per-tube heat-flux values given in ref 5. Predictions of the reactor exit conditions by the model are compared with the industrial data in Table A3, which shows that the model based on the free-radical mechanism is quite accurate.

Nomenclature

A = frequency factor, s^{-1} or m^3 kmol^{-1} s^{-1}
A_t = tube cross-sectional area, m^2
C_j = concentration of species j in gas mixture, kmol/m^3
$C_{p,j}$ = specific heat capacity of species j, kJ kmol^{-1} K^{-1}
d_{in} = tube internal diameter, m
E = activation energy, kcal/kmol
F = total molar flow rate of all species other than steam, kmol/s
F_{steam} = molar flow rate of steam, kmol/s
F_T = total molar flow rate of gas mixture including steam, kmol/s
F_r = friction factor, m^{-1}
f = mass flow rate, kg/s
g_c = Newton's conversion factor, 1000 kg m kN^{-1} s^{-2}
G_m = mass flux of the gas mixture, kg m^{-2} s^{-1}

I = minimization function
J = maximization function
k_i = kinetic parameter for reaction i, s^{-1} or m^3 kmol^{-1} s^{-1}
L = reactor length
M_j = molecular weight of species j, kg/kmol
M_m = molecular weight of gas mixture, kg/kmol
n_{tubes} = number of tubes in a radiant coil
P = pressure, kPa
p_m = probability of mutation for real-coded variables
$p_{m,b}$ = probability of mutation for binary-coded variables
p_c = probability of crossover
$q(x)$ = heat flux at length x of the reactor, kW/m^2
R = ideal gas constant, 8.314 51 J mol^{-1} K^{-1}
R_b = bend radius, m
R_s = seed for random number generator
Re = Reynolds number
r_i = rate of reaction i, kmol m^{-3} s^{-1}
S = selectivity
SR = steam-to-ethane mass ratio
T = temperature, K
t_r = residence time, s
X = conversion of ethane
x_i = mole fraction of species i

Greek Symbols

$\Delta H_{f,j}$ = heat of formation of species j, kJ/kmol
$\Delta H_{f,j}^{\circ}$ = heat of formation of species j at the reference temperature, 298 K, kJ/kmol
Λ = angle described by the bend, taken to be 180° here
α = heat-flux parameter, kW/m^2
α_{ij} = stoichiometric coefficient of species j in reaction i
β = heat-flux parameter, kW/m^2
γ = heat-flux parameter, kW/m^2
η_c = distribution index for the simulated crossover operation
η_m = distribution index for the simulated mutation operation
μ = viscosity of gas, kg m^{-1} s^{-1}
μ_m = viscosity of gas mixture, kg m^{-1} s^{-1}

Subscripts

avg = average
C_2H_4 = ethylene
i = reaction i
in = inlet
j = species j
kg = mass
ref = reference
x = distance from reactor entrance, m

Literature Cited

(1) Lacson, J.; Wong, S. CEH Report: Ethylene. In *Chemical Economics Handbook*; SRI Consulting: Menlo Park, CA, 2002 (accessed at http://ceh.sric.sri.com/Public/Reports/432.0000, Oct 2003).

(2) Ethylene Industry Outlook 220. In *Process Economics Program Report 220*; SRI Consulting: Menlo Park, CA (accessed at http://pep.sric.sri.com/Public/Reports/Phase_96/RP220/RP220.html, Oct 2003).

(3) Ethylene. In *Encyclopaedia of Chemical Processing and Design*; McKetta, J., Wesmantel, G. E., Eds.; John Wiley and Sons: New York, 1982; p 46.

(4) Ethylene. In *Ullmann's Encyclopedia of Industrial Chemistry*; Elvers, B., Hawkin, S., Russey, W., Eds.; John Wiley and Sons: New York, 1992.

(5) Froment, G. F.; Van de Steene, B. O.; Van Damme, P. S.; Narayanan, S.; Goossens, A. G. Thermal Cracking of Ethane and Ethane−Propane Mixtures. *Ind. Eng. Chem. Process Des. Dev.* **1976**, *15*, 495.

(6) Sundaram, K. M.; Froment, G. F. Modeling of Thermal Cracking Kinetics. 1. Thermal Cracking of Ethane, Propane and Their Mixtures. *Chem. Eng. Sci.* **1977**, *32*, 601.

(7) Froment, G. F.; Bischoff, K. B. *Chemical Reactor Analysis and Design*; John Wiley & Sons: New York, 1990.

(8) Sundaram, K. M.; Froment, G. F. Modeling of Thermal Cracking Kinetics. 3. Radical Mechanisms for the Pyrolysis of Simple Paraffins, Olefins, and Their Mixtures. *Ind. Eng. Chem. Fundam.* **1978**, *17*, 174.

(9) Pacey, P. D.; Purnell, J. H. *Ind. Eng. Chem. Fundam.* **1972**, *11*, 233.

(10) Siklos, P.; Balint, A.; Albright, L. F. *Acta Chim.-Hung.* **1983**, *114*, 79.

(11) Rangaiah, G. P.; Pang, N. S.; Tay, V. L. T. A Study of Kinetic Models for Simulating Industrial Ethane Cracking Reactors. Proceedings of the 4th Asian Pacific Confederation of Chemical Engineering (APCChE), Singapore, 1987.

(12) Froment, G. F.; Kinetics and Reactor Design in the Thermal Cracking for Olefins Production. *Chem. Eng. Sci.* **1992**, *47*, 2163.

(13) Heynderickx, G. J.; Froment, G. F. Simulation and Comparison of the Run Length of an Ethane Cracking Furnace with Reactor Tubes of Circular and Elliptical Cross Sections. *Ind. Eng. Chem. Res.* **1998**, *37* (3), 914.

(14) Rao, M. V. R.; Plehiers, P. M.; Froment, G. F. The Coupled Simulation of Heat Transfer and Reaction in a Pyrolysis Furnace. *Chem. Eng. Sci.* **1988**, *43*, 1223.

(15) Plehiers, P. M.; Froment, G. F. Firebox Simulation of Olefin Units. *Chem. Eng. Commun.* **1989**, *80*, 81.

(16) Dente, M.; Pierucci, S.; Ranzi, E. New Improvements in Modelling Kinetic Schemes for Hydrocarbons Pyrolysis Reactors. *Chem. Eng. Sci.* **1992**, *47*, 2629.

(17) Silva, C M.; Biscaia Jr, E. C. Genetic algorithm development for multi-objective optimization of batch free-radical polymerization reactors. *Comput. Chem. Eng.* **2003**, *27*, 1329.

(18) Srinivas, N.; Deb, K. Multi-Objective Function Optimization Using Non-Dominated Sorting Genetic Algorithms. *Evol. Comput.* **1995**, *2*, 221.

(19) Goldberg, D. E. *Genetic Algorithms in Search, Optimization and Machine Learning*; Addison-Wesley: New York, 1989.

(20) Mitra, K.; Deb, K.; Gupta, S. K. Multi-Objective Dynamic Optimization of an Industrial Nylon-6 Semi-batch Reactor Using Genetic Algorithm, *J. Appl. Polym. Sci.* **1998**, *69*, 69.

(21) Rajesh, J. K.; Gupta, S. K.; Rangaiah, G. P.; Ray, A. K. Multi-Objective Optimization of Industrial Hydrogen Plants. *Chem. Eng. Sci.* **2001**, *56*, 999.

(22) Deb, K.; Gulati, S. Design of truss-structures for minimum weight using genetic algorithms. *J. Finite Elements Anal. Des.* **2001**, *37*, 447.

(23) Yee, A. K. Y.; Ray, A. K.; Rangaiah, G. P. Multi-objective optimization of an industrial styrene reactor. *Comput. Chem. Eng.* **2003**, *27*, 111.

(24) Deb, K.; Pratap, A.; Agarwal, S.; Meyarivan, T. A Fast and Elitist Multi-Objective Genetic Algorithm: NSGA-II. *IEEE Trans. Evol. Comput.* **2002**, *6*, 182.

(25) Deb, K.; Agrawal, R. B. Simulated Binary Crossover for Continuous Search Space. *Complex Syst.* **1995**, *9*, 115.

(26) Tarafder, A.; Ray, A. K.; Rangaiah, G. P. Application of Nondominated Sorting Genetic Algorithms for Multi-objective Optimization of an Industrial Styrene Reactor. Proceedings of the 2nd International Conference on Computational Intelligence, Robotics and Autonomous Systems, Singapore, Dec 15−18, 2003.

(27) Kasat, R. B.; Kunzru, D.; Saraf, D. N.; Gupta, S. K. Multiobjective optimization of industrial FCC unit using elitist nondominated sorting genetic algorithm. *Ind. Eng. Chem. Res.* **2002**, *41*, 4765.

(28) Nandasana, A.; Ray, A. K.; Gupta, S. K. Dynamic model of an industrial steam reformer and its use for multiobjective optimization. *Ind. Eng. Chem. Res.* **2003**, *42*, 4028.

(29) Deb, K.; Mitra, K.; Dewri, R.; Majumdar, S. *Towards a Better Understanding of the Epoxy Polymerisation Process Using Multi-objective Evolutionary Computation*; KanGAL Report No. 2004001; Kanpur Genetic Algorithm Laboratory: Kanpur, India, 2004 (available at http://www.iitk.ac.in/kangal/pub.htm).

(30) Deb, K. Unveiling innovative design principles by means of multiple conflicting objectives. *Eng. Optim.* **2003***, 35*, 445.

(31) Knudsen, J. G.; Katz, D. L. *Fluid Dynamics and Heat Transfer*; McGraw-Hill: New York, 1958.

(32) Nekrasov, B. B. *Hydraulics*; Peace Publishers: Moscow, USSR, 1969.